The exceptionally high reactivity of Cys 621 is critical for electrophilic activation of the sensory nerve ion channel TRPA1

Parmvir K. Bahia,[1] Thomas A. Parks,[1] Katherine R. Stanford,[1] David A. Mitchell,[2] Sameer Varma,[3] Stanley M. Stevens Jr.,[3] and Thomas E. Taylor-Clark[1]

[1]Department of Molecular Pharmacology and Physiology and [2]Department of Molecular Medicine, Morsani College of Medicine, University of South Florida, Tampa, FL 33612

[3]Department of Cell Biology, Microbiology, and Molecular Biology, College of Arts and Sciences, University of South Florida, Tampa, FL 33620

Activation of the sensory nerve ion channel TRPA1 by electrophiles is the key mechanism that initiates nociceptive signaling, and leads to defensive reflexes and avoidance behaviors, during oxidative stress in mammals. TRPA1 is rapidly activated by subtoxic levels of electrophiles, but it is unclear how TRPA1 outcompetes cellular antioxidants that protect cytosolic proteins from electrophiles. Here, using physiologically relevant exposures, we demonstrate that electrophiles react with cysteine residues on mammalian TRPA1 at rates that exceed the reactivity of typical cysteines by 6,000-fold and that also exceed the reactivity of antioxidant enzymes. We show that TRPA1 possesses a complex reactive cysteine profile in which C621 is necessary for electrophile-induced binding and activation. Modeling of deprotonation energies suggests that K620 contributes to C621 reactivity and mutation of K620 alone greatly reduces the effect of electrophiles on TRPA1. Nevertheless, binding of electrophiles to C621 is not sufficient for activation, which also depends on the function of another reactive cysteine (C665). Together, our results demonstrate that TRPA1 acts as an effective electrophilic sensor because of the exceptionally high reactivity of C621.

The Journal of General Physiology

INTRODUCTION

Mammalian TRPA1 is a tetrameric cation channel expressed on nociceptive sensory nerve membranes that plays an important role in initiating nociceptive responses and pain to oxidative stress (Bandell et al., 2004; Jordt et al., 2004). TRPA1 is directly activated by electrophiles (e.g., 4-hydroxynonenal, cinnamaldehyde, and iodoacetamide [IA]) capable of covalent modification of cysteines (Hinman et al., 2006; Macpherson et al., 2007a,b; Trevisani et al., 2007; Taylor-Clark et al., 2008a,b, 2009). Nociceptive responses to electrophiles are likely an adaptation to the destructive reactions of electrophiles with DNA and proteins resulting in dysfunction (Marnett et al., 2003).

Oxidative stress and subsequent endogenous electrophile production is a major threat to aerobic cells, and thus protective strategies have developed (Halliwell, 1999). In particular, eukaryotic cells contain millimolar glutathione (GSH), a Cys-containing tripeptide that reacts with electrophiles. The GSH–electrophile reaction is also accelerated by multiple enzymes, such as glutathione-S-transferase (Hayes et al., 2005; Brigelius-Flohé and Flohé, 2011). Therefore, this detoxifying system protects Cys residues in other proteins. As such, electrophile sensors (e.g., TRPA1) must be able to detect electrophiles within the accelerated antioxidant environment: sensor–electrophile reactions must compete with existing reactions. This is particularly important for nociceptive signaling that initiates responses in seconds to stimuli that are simply potentially noxious; i.e., effective nociceptive signaling evokes action before catastrophic injury.

Electrophiles activate TRPA1 expressed in either nociceptive neurons or in heterologous systems within seconds (Bandell et al., 2004; Jordt et al., 2004; Hinman et al., 2006; Macpherson et al., 2007a,b; Trevisani et al., 2007; Nassenstein et al., 2008; Taylor-Clark et al., 2008a,b, 2009), suggesting a covalent modification rate rivaling the fastest antioxidant enzymes. It is likely that the unknown mechanisms underlying the rapid reaction rates are fundamental to TRPA1's ability to competently sense electrophilic danger. Until now, studies have focused solely on outcomes of TRPA1 activation, which a priori include mechanisms involved in both binding and channel gating. As such, the mechanisms underlying electrophile sensing by TRPA1 are uncertain, although single channel recordings indicate that this functionality is intrinsic to TRPA1. Under physiological conditions, electrophilic activators of TRPA1

Correspondence to Thomas E. Taylor-Clark: ttaylorc@health.usf.edu

Abbreviations used in this paper: ABC, ammonium bicarbonate; AITC, allyl isothiocyanate; CAM, carbamidomethylation; GSH, glutathione; HBS, HEPES-buffered saline; IA, iodoacetamide; MS, mass spectrometry; NEM, *n*-ethylmaleimide; NMM, *n*-methylmaleimide; ROI, region of interest; TNB, 2-nitro-5-thiobenzoate.

The Rockefeller University Press $30.00
J. Gen. Physiol. 2016 Vol. 147 No. 6 451–465
www.jgp.org/cgi/doi/10.1085/jgp.201611581

such as 4-hydroxynonenal and IA only modify nucleophilic Cys's (Doorn and Petersen, 2002; Mendoza and Vachet, 2009). Mutation studies have suggested Cys's (e.g., C414, C621, and C665) are critical to TRPA1 activation by electrophiles (Hinman et al., 2006; Macpherson et al., 2007a; Takahashi et al., 2008), although it is not clear whether these Cys's are involved (directly or indirectly) with binding or activation. Previous studies have suggested that TRPA1 can be covalently modified at most intracellular Cys's (Macpherson et al., 2007a; Wang et al., 2012), although these qualitative studies used excess electrophile exposures that would bind nonreactive and reactive Cys's alike. Lastly, intracellular polyphosphates are required for TRPA1 activation (Kim and Cavanaugh, 2007), but their role in electrophilic binding has not been investigated. Thus, it is unclear which factors determine the apparently extraordinary reaction rate of TRPA1 to electrophiles and also how binding leads to activation. Moreover, some orthologues (e.g., rattlesnake) are nonresponsive to electrophiles despite possessing many of the same Cys's that have been identified as key sites in mammalian TRPA1 (Cordero-Morales et al., 2011). Thus, it is unclear whether these differential responses represent differences in electrophilic binding or downstream activation mechanisms.

Here, we use physiologically relevant exposures in binding studies and functional experiments to offer mechanistic insights into the functional responses of TRPA1 to electrophiles. We demonstrate that TRPA1 possesses a complex reactive Cys profile centering on the extraordinary reactivity of C621, which is dependent on its neighbor K620, and that is necessary for electrophile-induced activation. C665 only marginally contributes to electrophilic adduction but is required for electrophile-induced activation.

MATERIALS AND METHODS

Spectrophotometric assays of thiol chemistry

Reactions were performed in 0.1 M phosphate buffer (at pH 7.4) containing 1 mM EDTA at room temperature and measured using a Jenway 6405 scanning spectrophotometer. Unreacted cinnamaldehyde and IA were detected at 290 nm (Chen and Armstrong, 1995), molar absorptivity of 18,463 $M^{-1}cm^{-1}$ and 227 $M^{-1}cm^{-1}$, respectively. Cinnamaldehyde or IA was reacted with excess (4.3 mM) GSH (negligible absorption at 290 nm), and the loss of absorption at 290 nm was followed. The natural log of [unreacted electrophile] was plotted against time, and the slope (s^{-1}) of the straight line was calculated. Given that [electrophile] << [GSH], the second order reaction rate ($M^{-1}s^{-1}$) for each reaction was calculated by dividing the slope by [GSH]. Activated Thiopropyl Sepharose (Han et al., 1999) was reacted with 50 µM DTNB to produce 100 µM 2-nitro-5-thiobenzoate (TNB), which was detected at 412 nm, molar absorptivity of 14,140 $M^{-1}cm^{-1}$. Reaction of TNB with IA, *n*-ethylmaleimide (NEM), and *n*-methylmaleimide (NMM) was performed in 0.1 M phosphate buffer (at pH 7.4) containing 1 mM EDTA at room temperature, in some cases also including 5 mM GSH, and measured at 412 nm. The natural log of [unreacted TNB] was plotted against time, and the slope (s^{-1}) of the straight line was calculated. Given that [TNB] << [electrophile], the second order reaction rate ($M^{-1}s^{-1}$) for each reaction was calculated by dividing the slope by [electrophile].

V5-tagged constructs, mutations, and expression in HEK293 cells

Plasmids containing full-length TRPA1 genes were the gifts of D. Julius (University of California, San Francisco, San Francisco, CA; human or hTRPA1) and A. Patapoutian (Scripps Research Institute, La Jolla, CA: mouse or mTRPA1). hTRPV1 was obtained from the Center for Personalized Diagnostics via the DNASU Plasmid Repository (HsCD00731917). The plasmid containing full-length redox-sensitive green fluorescent protein 1 (roGFP) was a gift from J. Remington (University of Oregon, Eugene, OR). TRP channel genes were subcloned into pcDNA3.1 V5-His-TOPO or pcDNA3.1D V5-His-TOPO (Thermo Fisher Scientific) using primers (Biosynthesis) containing restriction sites allowing ligation into one or other vector. Point mutations were made by PCR. TRP channels and roGFP were expressed in HEK293 cells (cultured in Dulbecco's modified Eagle's medium supplemented with 10% FBS, 100 U/ml penicillin, and 100 µg/ml streptomycin) using Lipofectamine 2000 (Thermo Fisher Scientific). mTRPA1 cultures were supplemented with 5 µM ruthenium red.

Calcium imaging

Cells were studied for changes in $[Ca^{2+}]_i$ with 8 µM Fura-2AM. For imaging, cells were superfused with HEP ES-buffered saline (HBS; composition [mM]: 154 NaCl, 4.7 KCl, 1.2 $MgCl_2$, 2.5 $CaCl_2$, 10 HEPES, and 5.6 dextrose adjusted to pH 7.4 with NaOH) for 10 min before and throughout each experiment. Changes in $[Ca^{2+}]_i$ were monitored by sequential dual excitation, 340 and 380 nm (emission 510 nm), measured by digital microscopy (CoolSNAP HQ2; Photometrics) and analyzed by specialized software (Nikon Elements; Nikon). Cells were exposed to 5 µM ionomycin (for 60 s) to obtain a maximal response. For the analysis of $[Ca^{2+}]_i$, we used the excitation ratio 340 nm/380 nm and related all measurements to the peak positive response in each cell. This approach bypasses the conversion of ratiometric responses into absolute $[Ca^{2+}]_i$ using Tsien parameters (Taylor-Clark et al., 2015). At each time point, each cell was normalized to its maximum $[Ca^{2+}]_i$ (evoked by the Ca^{2+} ionophore ionomycin). Data were presented as the percentage change in 340/380 ratio (R): response at

time (x) = 100 × (R_x − R_{bl})/(R_{max} − R_{bl}), where R_x was the 340/380 ratio of the cell at a given time point, R_{bl} was the cell's mean baseline 340/380 ratio measured over 60 s, and R_{max} was the cell's peak 340/380 ratio. Only cells that had low $[Ca^{2+}]_i$ at baseline (R < 1.3) and yielded a robust response to the positive control were included in analyses. TRPA1 expression was determined by a positive response to either 100 µM IA or 100 µM cinnamaldehyde or 200 µM thymol. The rate of TRPA1 activation was calculated for each cell from the normalized response against time data. This was based on the assumption that the [electrophile] >>> [functional TRPA1 groups], that electrophilic binding was irreversible, and that the maximum response correlated with maximum binding of functional groups on TRPA1. The time to half maximum ($t_{1/2}$) was calculated for each cell. The second order rate for the reaction (assuming pseudo-first order conditions) in $M^{-1}s^{-1} = 1/((t_{1/2})/\ln(2))$ * [electrophile].

Cytosolic redox assay using roGFP

HEK293 cells expressing roGFP were superfused with HBS. Changes in cytosolic redox state were monitored by sequential dual excitation, 405 and 470 nm (emission 525 nm). 300 µM H_2O_2 was applied to cause an oxidation-induced increase in roGFP 405/470 ratio. The difference (Δ) between baseline ratio and the maximum response to H_2O_2 was quantified to represent the responsiveness of roGFP to oxidation.

Electrophile binding of TRP

HEK293 transfected with V5-tagged TRP channels were lifted with Accutase (Innovative Cell Technologies, Inc.), spun down for 2 min at 700 *g*, and resuspended in 250 µl to 1 ml of PBS. BODIPY 507/545 IA (B-IA; Molecular Probes) was added to the PBS–cell suspension. The B-IA–binding reaction was stopped by flooding with 15 ml of 1 mM IA and spun down, and the flooding repeated a second time. Cells were then resuspended in lysis buffer (50 mM TRIS, 150 mM NaCl, 2% Triton X-100, and 0.05% SDS) containing protease inhibitors (Complete Mini; Roche) and then left on ice for 30 min to solubilize protein. Lysates were spun down at 14,000 *g* for 15 min to remove debris.

Permeabilization with saponin. For experiments requiring changes in the intracellular milieu, cells were resuspended in buffer containing 50 µg/ml saponin. Saponin selectively dissolves plasma membrane cholesterol, resulting in permeabilization of intact cells (Jamur and Oliver, 2010). The cells were left for 3 min at room temperature to permeabilize and for the intra- and extracellular solutions to equilibrate.

Effects of pH on B-IA binding. The different pH ranges for phosphate-citrate buffer (PB) were achieved by adding 0.1 M citric acid to 0.2 M Na_2HPO_4 and confirmed using a pH meter. HEK293 cells expressing hTRPA1 were initially resuspended in (pH 7.4) PBS or PBS containing 100 µM IA and incubated at room temperature for 7 min. They were then spun down and resuspended in PB (buffered to pH 5.0 or 7.4) containing 50 µg/ml saponin for 3 min before B-IA treatment.

Immunoprecipitation and Western blotting. All TRP channels were immunoprecipitated and detected in Western blot using the same primary antibody targeting an identical V5 epitope in each construct. 25 µl Dynabeads G (Thermo Fisher Scientific) was resuspended in PBS in 0.02% Tween 20. 1 µg anti-V5 antibody was added, and the bead–antibody complex was allowed to form by agitating at room temperature for 45 min. The antibody-containing supernatant was removed, and treated HEK cell lysates were incubated with the bead–antibody complex for 18 h at 4°C. Beads were washed in PBS with 0.02% Tween 20 and then boiled in RIPA buffer (100 mM TRIS, 150 mM NaCl, 1 mM EDTA, 1% Triton X-100, 1% Na deoxycholate, and 0.1% SDS) containing 1× Laemmli buffer for 10 min. Total immunoprecipitated protein eluate and the ECL Plex Fluorescent Rainbow markers (GE Healthcare) were then separated by 9% SDS-PAGE and transferred onto Hybond LFP PVDF membranes (GE Healthcare). Membranes were blocked in 1% bovine serum albumin in TRIS-buffered saline (TBS; 20 mM TRIS base and 500 µM NaCl). Membranes were then left in 1:2,500 anti-V5 mouse monoclonal antibody (made up in blocking buffer; R960-25; Thermo Fisher Scientific) for 18 h at 4°C. After three washes in TBS containing 0.025% Tween 20, membranes were incubated in a goat anti–mouse secondary antibody, Alexa Fluor 647 conjugate for 1 h at room temperature. All blots were scanned using a Typhoon 9410 imager (GE Healthcare): B-IA excitation at 488 nm, emission at 520 nm; 2° Alexa Fluor 647 excitation at 633 nm, emission at 670 nm.

B-IA assay data analysis. Band intensities of B-IA and Alexa Fluor 647 (TRP protein) signals were measured using ImageJ64 software (National Institutes of Health). A horizontal region of interest (ROI) was placed within the TRP band, and another ROI was placed below the band as a measure of the background. The same ROIs were used to analysis the B-IA fluorescence. The background (b) was subtracted from both, and then B-IA data were normalized to TRP protein (normalized data = (BIA − b)/(TRP − b)), thus allowing for comparisons of normalized B-IA binding across all TRP channel orthologues, paralogues, and mutants.

IA binding of hTRPA1 for mass spectrometry (MS). 50 million live HEK293 cells overexpressing V5-tagged hTRPA1 were treated with 30 µM IA for 2 min, then flooded with 1 mM NEM to quench the reaction for 7

min, and then lysed in the presence of protease inhibitors. Lysates were immunoprecipitated and separated by 6% SDS-PAGE. Two separate but identical experiments were performed on separate days.

In-gel digests. 6% SDS-polyacrylamide gels were stained with Coomassie blue to visualize protein gel bands and washed in distilled water to remove excess background stain. Protein bands were excised and destained with three 15-min washes in 50 mM ammonium bicarbonate (ABC) and 50% acetonitrile solution. Acetonitrile and 100 mM ABC were then used to dehydrate and rehydrate the gel pieces for 5 min. This was followed by 15 min in 1:1 acetonitrile and 100 mM ABC. To reduce disulfide bonds, 45 mM DTT was added for 30 min, and gels were left at 55°C. Free cysteines were alkylated with 50 mM NMM for 60 min. 100 µl of freshly prepared 100 ng/µl trypsin (sequencing grade modified; Promega) in 50 mM ABC was added to the samples, which were then digested at 37°C overnight. Digested peptides were extracted with 1:1 acetonitrile and 0.1% formic acid, dried, and dissolved in 0.1% formic acid solution for MS analysis.

MS

Digested peptides were desalted inline using either an Acclaim PepMap C18 Nano-Trap or a C4 sample trap (New Objective) and then separated on an Acclaim PepMap C18 (75 µm × 50 cm) UPLC column (Thermo Fisher Scientific) or on a CMP Scientific C4 (75 µm × 20 cm), respectively, using an EASY-nLC 1000 with a gradient time of 90 min (2–40% acetonitrile in 0.1% formic acid). Mass spectrometric analysis was performed on a hybrid quadrupole-Orbitrap instrument (Q Exactive Plus; Thermo Fisher Scientific), using a top 10 data–dependent acquisition method with a dynamic exclusion time of 20 s. Full scan and MS/MS resolution was 70,000 and 17,500, respectively. Peptide and protein identifications were assigned through MaxQuant (version 1.5.0.30) using the UniProt *Homo sapiens* database. Acetylation (protein N terminus) and oxidation of methionine were set as default variable modifications. Additional variable modifications included NEM (+125), NMM (+111), and carbamidomethylation (CAM [+57], after reaction with IA) of Cys residues. Other database search parameters included trypsin/P as the enzyme used with the possibility of two missed cleavages and 20 ppm (first search)/4.5 ppm (recalibrated second search) mass tolerance for precursor ions and 20 ppm mass tolerance for fragment ions. Further detection validation of modified Cys-containing peptides identified from data-dependent acquisition was performed using targeted MS/MS analysis. Targeted MS/MS analysis was performed at 17,500 mass resolution with an automatic gain control target value of 1e6 and maximum ion injection time of 200 ms. The inclusion list of all modified Cys-containing peptides for targeted MS/MS analysis was generated based on identified peptides from MaxQuant search results. Raw data can be found at CHO RUS Project (#1055).

For site-specific quantitation of Cys residues modified by IA, raw intensity values of Cys-containing peptides from MaxQuant were used to determine the amount of CAM at various sites in TRPA1. Specifically, a ratio of the sum of intensities of all modified versions of a particular carbamidomethylated peptide over the sum of intensities of all possible modified versions of that same peptide (e.g., oxidized methionine, NEM/NMM modification of Cys, etc.) was calculated. Note that the percentage of CAM binding is based on the assumption that ionization efficiencies are not significantly different between NEM-, NMM-, and CAM-modified versions of the same peptide. Although the absolute percentage of CAM may not be an exact value based on this assumption, the relative ranking of CAM percentage among Cys-containing peptides would still be an accurate approach to determine the highly reactive Cys residues in TRPA1. Two separate experiments were performed, each with duplicate mass spectrometric analyses performed. The first experiment used a C18 column; the second experiment used a C18 column for one analysis and a C4 column for the other analysis. Data are the mean across the two experiments. For each analysis, an identified peptide with the lowest intensity was used to approximate the limit of detection for the system. The sum of the intensities (CAM bound, NEM bound, and NMM bound) for each Cys was divided by the intensity of the limit of detection peptide to yield an approximate signal to noise ratio. To approximate reaction rates of each Cys, the natural log of the percentage of unreacted Cys after IA treatment was plotted against time, and the slope (s^{-1}) of the straight line was calculated. Given that [electrophile] <<< [individual Cys], the second order reaction rate (K_{obs}, $M^{-1}s^{-1}$) for each reaction was calculated by dividing the slope by [IA].

Quantum mechanical simulations of cysteine deprotonation

The effect of a functional group X = {NH_4^+, $HCOO^-$, CH_4} on the deprotonation energy of Cys is determined as $\Delta\Delta E = E(Cys^-,X) - E(CysH,X) - E(Cys^-) + E(CysH)$. Here, $E(Cys^-,X)$ and $E(Cys^-)$ are the electronic energies of a deprotonated Cys in the presence and absence of X, and $E(CysH,X)$ and $E(CysH)$ are the electronic energies of a protonated form of Cys in the presence and absence of X. These energies were determined using the hybrid B3LYP (Lee et al., 1988; Becke, 1993) density functional theory implemented in the Gaussian09 suite of programs (Gaussian, Inc.). The reported energies correspond to the single point values estimated for the relaxed geometries. The 3-D geometries were relaxed with positional constraints on the S atom of Cys,

N atom of NH_4^+, C atom of $HCOO^-$, and the C atom of CH_4 to maintain distances between Cys and the different functional groups. The effect of the solvent (ε = 78.54) was modeled using the polarizable continuum model (PCM) with the integral equation formalism variant (Cancès et al., 1997) and with a solvent radius of 1.4 Å. Electron densities of all atoms were expanded on 6-311++G** basis sets. For a subset of cases, we also compared estimates from this approach against the CBS-QB3 approach, an approach that belongs to the family of the complete basis set (CBS) methods of Montgomery et al. (1999). For functional groups placed at a distance of 6 Å, we found that the CBS-QB3 approach yields $\Delta\Delta E_{NH_4}$ = −1.8 kcal/mol, $\Delta\Delta E_{HCOO}$ = 1.6 kcal/mol, and $\Delta\Delta E_{CH_4}$ = 0.3 kcal/mol. These values are quantitatively comparable with those obtained from the B3LYP/6-311++G** approach, where $\Delta\Delta E_{NH_4}$ = −1.9 kcal/mol, $\Delta\Delta E_{HCOO}$ = 1.5 kcal/mol, and $\Delta\Delta E_{CH_4}$ = 0.3 kcal/mol.

Immunocytochemistry

For Nrf2 translocation experiments, HEK293 were (a) treated with HBS for 60 min, (b) treated with 1 mM IA (made in HBS) for 60 min, or (c) treated with 30 µM IA (made in HBS) for 2 min and then washed in HBS for 60 min. All treatments were performed at 37°C for the duration of the experiment. Cells were then immediately fixed in 4% paraformaldehyde, washed once in cold PBS, and then permeabilized in PBS containing 0.1% Triton X-100 (all steps were performed at room temperature for 10 min). Cells were then blocked in PBS with 0.025% Tween 20 (PBST) containing 1% BSA. After blocking for 1 h at room temperature, cells were incubated in 1:200 anti-Nrf2 primary antibody (C20; Santa Cruz Biotechnology, Inc.) made up in blocking buffer, overnight at 4°C. After three washes in PBST, cells were incubated in 1:500 of the donkey anti–rabbit Alexa Fluor 546–conjugated secondary (Thermo Fisher Scientific) at room temperature for 1 h. After three washes in PBST, the coverslips were mounted onto glass slides using Vectashield hard-set mounting medium either with or without DAPI (Vector Laboratories). Images were captured using an FV1000 MPE multiphoton laser-scanning microscope (Olympus) and analyzed with ImageJ (National Institutes of Health), with straight line ROI drawn from outside of each cell through the cytosol into the nucleus. The fluorescence intensity of the anti-Nrf2 signal was calculated for the background (b), cytosol (c), and nucleus (n). The normalized cytosolic/nuclear ratio was calculated for each cell thusly: $(c - b)/(n - b)$.

For TRP construct expression experiments, constructs were expressed in HEK293 cells that were incubated in 1 mM CellTracker green CMFDA (Thermo Fisher Scientific) for 15 min at 37°C. Cells were then fixed, permeabilized, and blocked as described for the Nrf2 immunohistochemical experiments. V5-tagged TRP proteins were detected with an anti-V5 primary antibody (R960-25, 1:5,000; Thermo Fisher Scientific) and the goat anti–mouse Alexa Fluor 647–conjugated secondary antibody (1:1,000).

Statistics

Data are presented as mean (±SEM where appropriate). Data derived from spectrophotometric experiments of electrophilic reactions, Fura-2AM functional experiments, B-IA–binding experiments, and Nrf2 translocation experiments yielded Gaussian distributions. In particular, similar variances were noted between B-IA–binding datasets. Two sets of unpaired data were compared with a one-tailed Student's *t* test, using $P < 0.05$ as significant.

Online supplemental material

Fig. S1 shows unreacted cinnamaldehyde and IA absorbance at 290 nm. Fig. S2 shows that IA-induced increase in cytosolic [Ca^{2+}] in hTRPA1-expressing HEK293 is entirely dependent on Ca^{2+} influx. Fig. S3 shows that B-IA activates and binds hTRPA1. Fig. S4 shows a graphical representation of MS coverage of hTRPA1 after trypsin digest. Fig. S5 shows examples of annotated MS/MS for IA adduction of hTRPA1 residues. Fig. S6 shows the calculated reaction rate of IA with C273, C621, C665, and C1085 normalized to the rate for C540. Fig. S7 shows that rapid IA treatment causes minor activation of the Keap1-Nrf2 system. Fig. S8 shows immunocytochemistry of hTRPA1 constructs. Fig. S9 shows that K620 is required for the apparent low pK_a of hTRPA1-reactive Cys. Online supplemental material is available at http://www.jgp.org/cgi/content/full/jgp.201611581/DC1.

RESULTS

Electrophiles activate hTRPA1 faster than they react with canonical Cys

Membrane-permeable electrophiles cinnamaldehyde and IA both absorb at 290 nm (Fig. S1). This absorbance disappears upon reaction with Cys in GSH (Fig. 1, A and B). We compared the kinetics of 50 µM cinnamaldehyde activation of hTRPA1 expressed in HEK293 cells with cinnamaldehyde's reaction with 5 mM GSH. Complete activation of hTRPA1 occurred within 70 s of cinnamaldehyde treatment, whereas only 50% of cinnamaldehyde had reacted with GSH by 670 s (Fig. 1 A). Similarly, 200 µM IA activated hTRPA1 at a much faster rate than IA's reaction with GSH (Fig. 1 B). We confirmed the slow reaction rate of IA with sulfhydryl groups using 100 µM TNB, a molecule whose absorbance at 412 nm (Fig. 1 C) decreases after reaction with electrophiles. Within 60 s, 30 µM IA reacted with <0.5% of the TNB (Fig. 1, D and E). Higher concentrations of IA and other electrophiles such as NEM and NMM re-

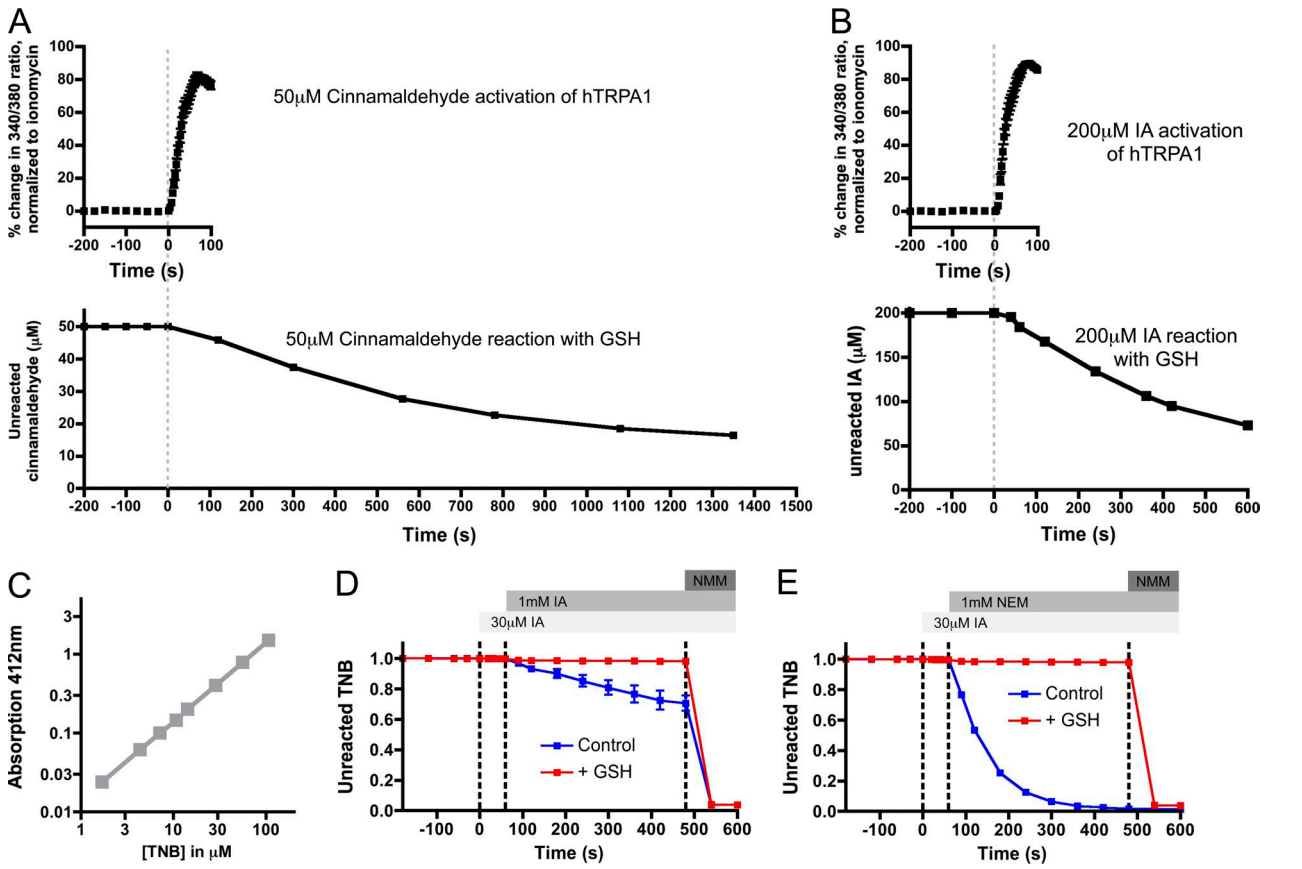

Figure 1. **Electrophiles activate hTRPA1 faster than they react with conventional sulfhydryl groups in vitro.** (A) 50 µM cinnamaldehyde activation of hTRPA1 in HEK293 (top, *n* = 28) and 50 µM cinnamaldehyde reaction with 5 mM GSH (bottom, *n* = 3). (B) 200 µM IA activation of hTRPA1 in HEK293 (top, *n* = 96) and its reaction with 5 mM GSH (bottom, *n* = 3). (A and B) Error bars denote SEM. (C) Absorbance of TNB at 412 nm. (D) Mean ± SEM loss of 100 µM TNB absorption at 412 nm after sequential reaction with 30 µM IA, 1 mM IA, and 100 mM NMM in control conditions (*n* = 3) and in the presence of 5 mM GSH (*n* = 3). (E) Mean ± SEM TNB loss after reaction with 30 µM IA, 1 mM NEM, and 100 mM NMM in control (*n* = 3) and with 5 mM GSH (*n* = 3). Error bars are too small to see on this scale.

acted significantly with TNB, with 1 mM NEM reacting 10 times faster than 1 mM IA (Fig. 1, D and E). GSH, at a typical cytosolic concentration (5 mM), inhibited the electrophile–TNB reaction as the result of preferential binding of the electrophiles with the excess thiol.

To determine the kinetics of electrophilic modification of Cys within the cell cytosol, we studied fluorescent changes in roGFP expressed in HEK293 upon oxidation by H_2O_2. 300 µM H_2O_2 caused an increase in the roGFP 405/488 ratio, as the result of the formation of a critical disulfide bond (Fig. 2 A; Dooley et al., 2004). As such, prior electrophilic modification of roGFP Cys would render it insensitive to H_2O_2. Indeed, treatment with 1 mM NEM for 420 s prevented H_2O_2-induced roGFP responses (Fig. 2, A–C). Treatment with 30 µM IA for 60 s had no effect on H_2O_2-induced roGFP responses (Fig. 2, B and C), again suggesting little covalent modification of Cys (on roGFP) with this rapid IA treatment.

In comparison, we found that ≥1 µM IA caused significant activation of hTRPA1-mediated Ca^{2+} transients in HEK293 (Fig. 2 D), and the time to half maximum activation ($t_{1/2}$) decreased as [IA] increased (Fig. 2 E). As expected, IA had no effect on cytosolic [Ca^{2+}] in nontransfected HEK293 and in TRPA1-transfected HEK293 in the absence of extracellular Ca^{2+}, thus confirming the specific role of TRPA1 channels on the IA-induced Ca^{2+} transients (Fig. 2 D and Fig. S2). We calculated the apparent second order rate constant for hTRPA1 activation to be 500–900 $M^{-1}s^{-1}$ (Fig. 2, E and F), which was dramatically quicker than IA's reaction with either GSH (0.4 $M^{-1}s^{-1}$) or TNB (1.3 $M^{-1}s^{-1}$; Fig. 2 F). Cinnamaldehyde-induced hTRPA1 activation was also dramatically quicker than its reaction with either GSH or TNB (Fig. 2 F). These data demonstrate the fundamental difference in the kinetics of electrophilic activation of hTRPA1 compared with electrophilic reaction with conventional sulfhydryl groups.

Mammalian TRPA1 possesses a "reactive" Cys subpopulation

We investigated the kinetics of electrophilic binding of hTRPA1 using fluorescently tagged B-IA. B-IA activated

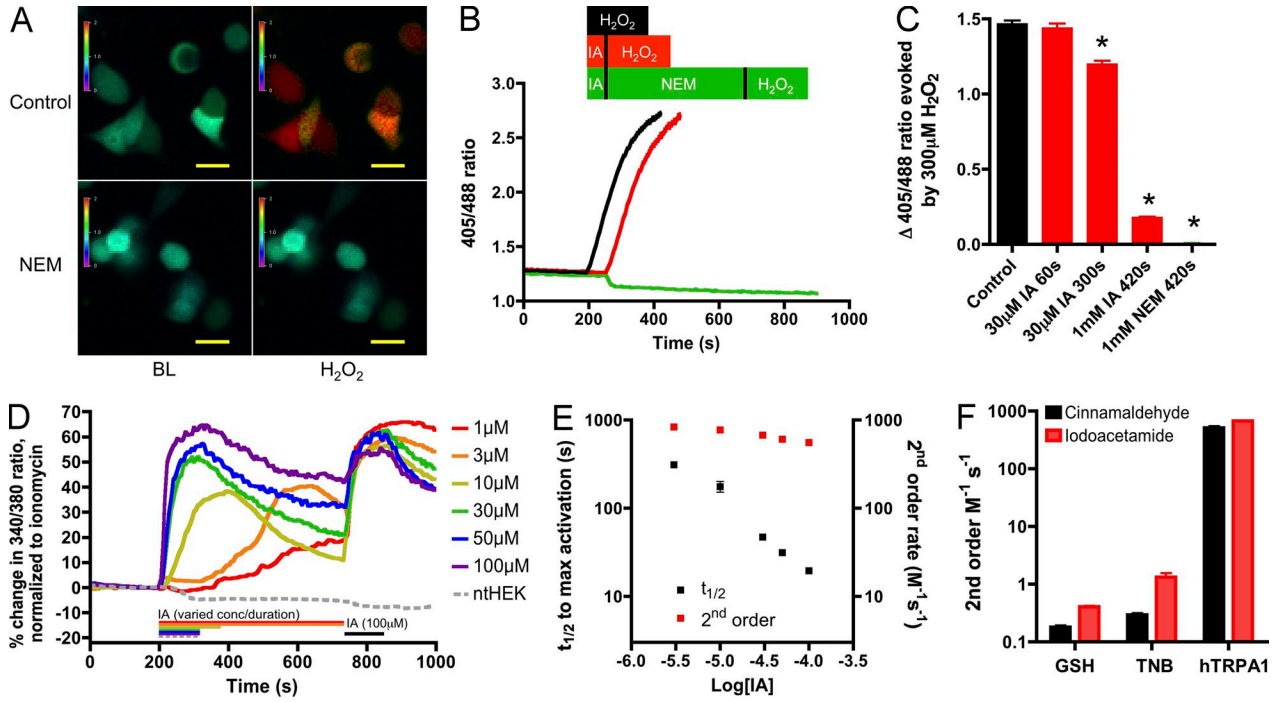

Figure 2. **Electrophiles activate hTRPA1 faster than they react with cytosolic sulfhydryl groups.** (A and B) 300 µM H_2O_2 causes an oxidation-induced increase in roGFP 405/470 ratio in HEK293 (n = 327), prevented by pretreatment with 1 mM NEM (420 s, n = 106) but not by 30 µM IA (60 s, n = 189). Bars, 20 µm. (C) Mean ± SEM H_2O_2-induced change in 405/470 ratio is reduced by electrophilic stimuli >30 µM IA (60 s; $n \geq 84$). *, $P < 0.05$. (D) IA activates hTRPA1 at [IA] ≥ 1 µM within 120 s. The dashed gray line denotes the response of nontransfected HEK293 to 100 µM IA (first and second stimuli); other colored lines denote hTRPA1-expressing HEK293 cells responding to varying [IA] (first stimulus) and 100 µM IA (second stimulus; $n \geq 36$). Colored bars denote the specific duration of each treatment: 1–3 µM (540 s), 10 µM (180 s), and ≥30 µM (120 s). (E) Increasing IA exposure activates hTRPA1 faster, yielding consistent second order reaction rates. (F) Comparison of second order rates for electrophilic modification of GSH (n = 3 each) and TNB ($n \geq 3$) and the activation of hTRPA1 ($n > 28$). (E and F) Error bars denote SEM.

hTRPA1 (Fig. S3 A) with an apparent second order rate of 640 $M^{-1}s^{-1}$. Using a modified rapid pulse-chase reaction, we exposed hTRPA1-expressing HEK293 cells to B-IA and then quenched the reaction with nonfluorescent IA. B-IA binding was normalized to hTRPA1 protein after background subtraction. Increasing B-IA concentrations or exposure times resulted in greater binding (Fig. 3, A and B). Two populations of B-IA–binding sites were observed: a rapidly bound and saturable population and a slowly bound population that under these conditions failed to saturate. It is likely that the former group includes Cys's critical for hTRPA1 activation, whereas the latter group likely comprises nonfunctional Cys's. As expected, B-IA binding to hTRPA1 was irreversible (Fig. S3 B).

Pretreatment of HEK293 expressing hTRPA1 with TRPA1 inhibitors HC-030031 and AP-18 (both 30 µM) failed to reduce B-IA binding (Fig. 3 C). However, pretreatment with nonfluorescent IA (100 µM, 10 min) reduced subsequent B-IA binding by 50%, suggesting that half of the B-IA binding was quenchable under these conditions (Fig. 3 C). Based on spectrophotometric analysis of the reaction of 5 µM TNB with 10-min treatment of 100 µM IA (Fig. 3 D), we predict that this particular IA exposure would react with ∼10% of conventional Cys's in hTRPA1. Thus, the difference between B-IA binding under control conditions and after IA pretreatment largely reveals the B-IA binding of "reactive" Cys.

Intracellular polyphosphates are required for TRPA1 activation by electrophiles (Kim and Cavanaugh, 2007). Using saponin, which selectively dissolves membrane cholesterol and dialyzes out soluble intracellular components (Jamur and Oliver, 2010), we found that native polyphosphates had no effect on B-IA binding (Fig. 3 E). Furthermore, supplementing saponin-treated HEK293 with 1 mM sodium polyphosphate also had no effect on B-IA binding.

We compared rapid B-IA binding of hTRPA1 with similar ion channels: mouse TRPA1 (mTRPA1), which is activated by electrophiles (Macpherson et al., 2007a); rattlesnake TRPA1 (rsTRPA1), which is not activated by electrophiles (Cordero-Morales et al., 2011); and human TRP vanilloid 1 (hTRPV1), the capsaicin-sensitive receptor that is also insensitive to electrophiles (Bautista et al., 2006). B-IA pulse-chase experiments were performed with and without pretreatment with untagged IA to reveal B-IA binding of reactive Cys. Con-

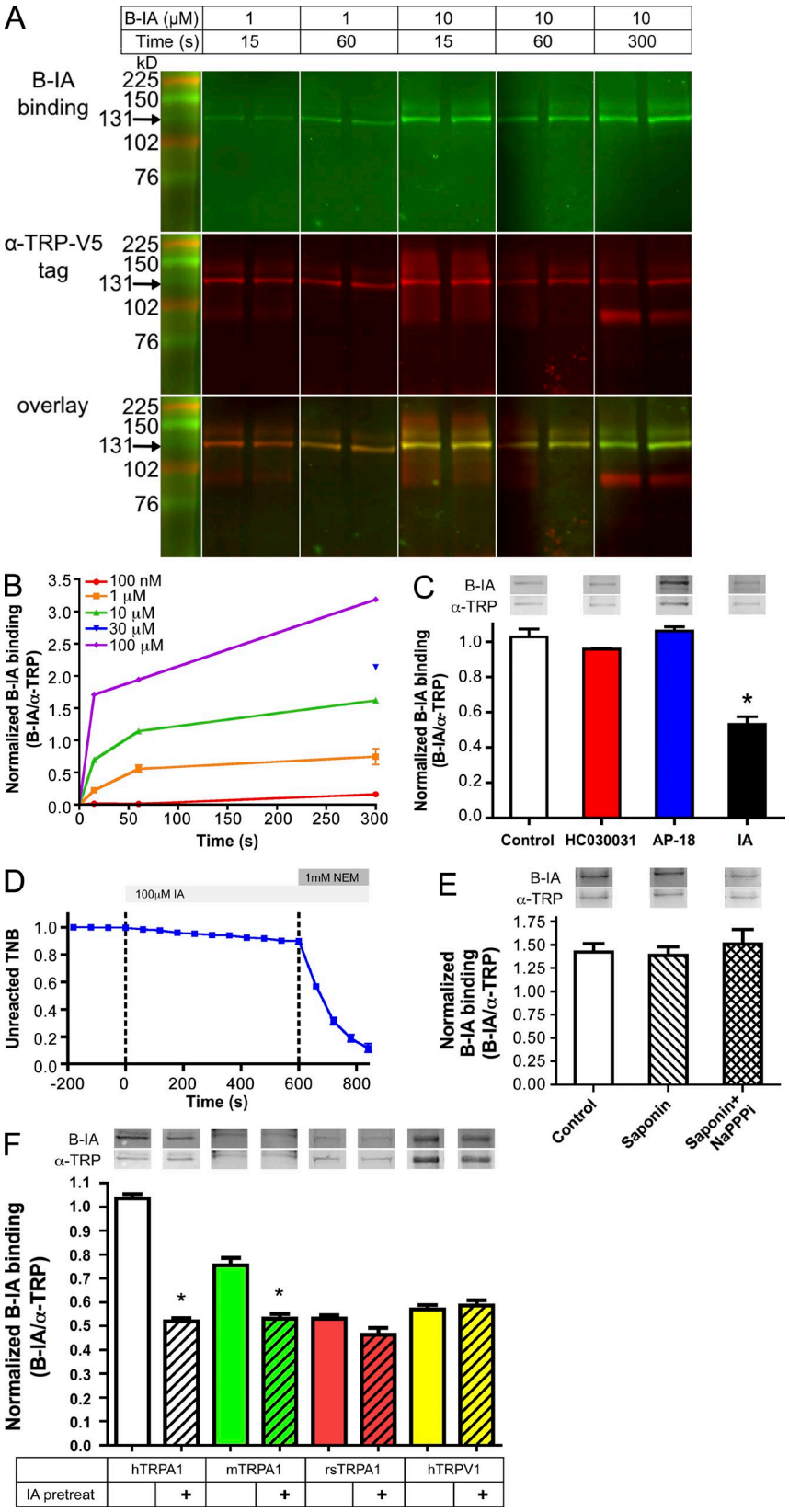

Figure 3. **B-IA covalently binds reactive groups in hTRPA1.** (A) Representative images of B-IA binding (green) on immunoprecipitated hTRPA1 quantified by the antibody against V5 tag (red). V5-tagged hTRPA1 had an expected mass of 131 kD. Overlay shows B-IA binding colocalizes with TRP channel. (B) Mean ± SEM for normalized B-IA binding on hTRPA1 ($n \geq 3$). (C) Normalized 10 μM B-IA binding to hTRPA1 (60 s) is reduced by pretreatment with unlabeled IA (100 μM, 10 min) but not by TRPA1 inhibitors HC030031 (30 μM) and AP-18 (30 μM; $n \geq 3$). The asterisk denotes difference from control (*, $P < 0.05$). (D) Mean ± SEM loss of 412-nm absorption after the reaction of 5 μM TNB with 100 μM IA (10 min) and 1 mM NEM ($n = 3$). (E) Normalized 10 μM B-IA binding to hTRPA1 (60 s) is unaffected by removal of intracellular polyphosphates (saponin) or by polyphosphate supplementation (saponin + NaPPPi; $n = 3$). (F) Normalized 10 μM B-IA (60 s) binding to hTRPA1, mTRPA1, rsTRPA1, and hTRPV1 ($n \geq 3$). Asterisks denote difference from control (clear bars) with IA pretreatment (100 μM, 10 min; hatched bars; *, $P < 0.05$). (C, E, and F) Error bars denote SEM. All bands in the blots are 131 kD, except for the yellow bars in F, which are 90 kD.

sistent with their sensitivity to electrophiles, mTRPA1 exhibited reactive Cys binding by B-IA, whereas rsTRPA1 and hTRPV1 only exhibited nonreactive B-IA binding (Fig. 3 F). Thus, our data indicate that a prerequisite for activation by electrophiles is the channel's capacity to rapidly react with electrophiles.

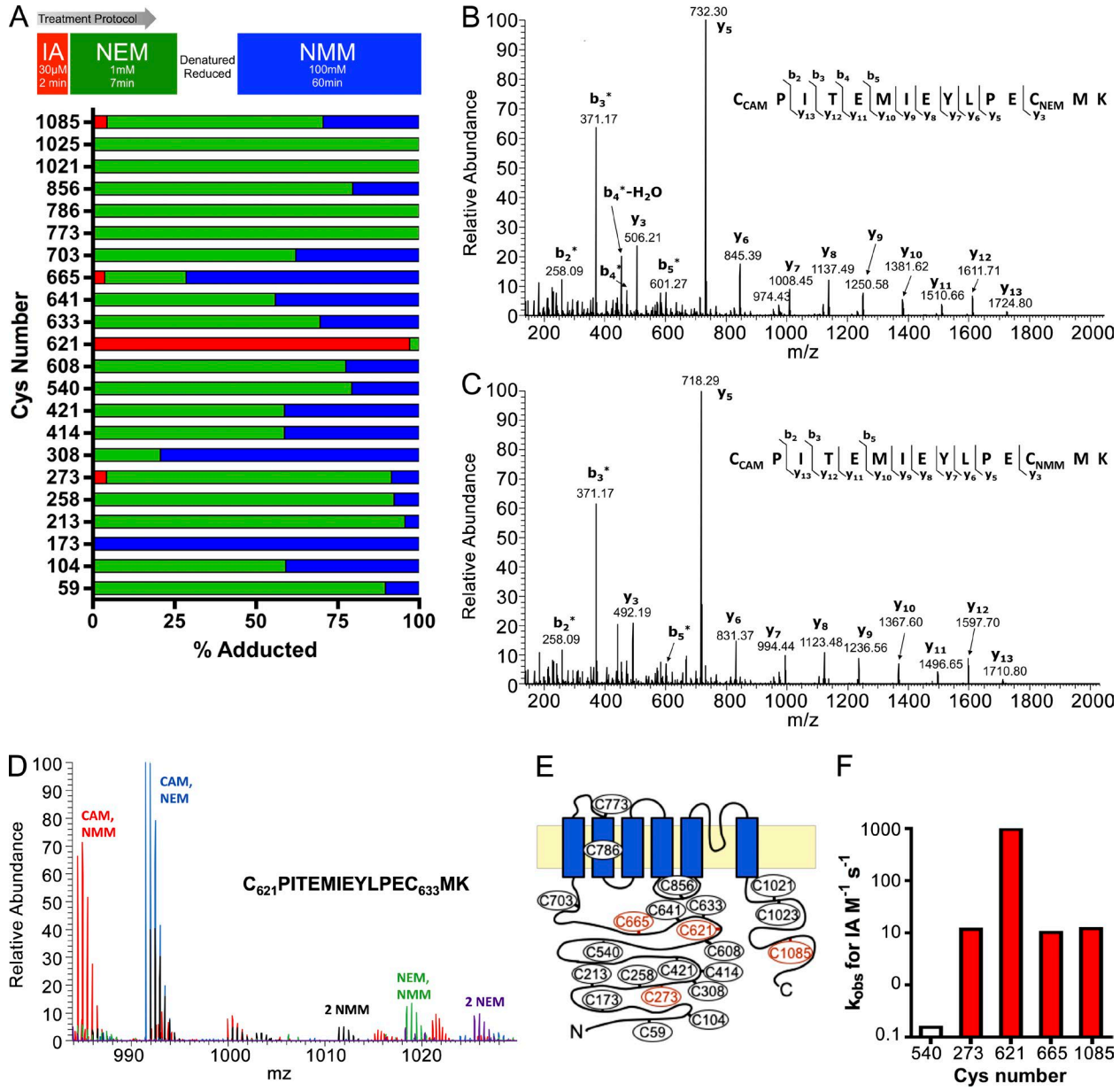

Figure 4. **hTRPA1 possesses four reactive Cys's.** (A, top) Treatment protocol for brief IA exposure of HEK293 cells expressing hTRPA1 for MS analysis. (bottom) Complete analysis of the percentage of each Cys adducted by IA, NEM, and NMM as determined by comparisons of identified MS/MS peaks. (B) Representative MS/MS spectra for tryptic peptide containing C621 (CAM modified) and C633 (NEM modified). (C) Representative MS/MS spectra for tryptic peptide containing C621 (CAM modified) and C633 (NMM modified). (B and C) Asterisks denote fragment ions with CAM modification. (D) Superimposed full scan mass spectra for the modified C621- and C633-containing tryptic peptide showing relative differences in peak intensity for each modified version (identified by different colors). Data are representative of the first analysis using a C18 column. Accurate mass-based (<5 ppm) reconstructed ion chromatograms were generated for each modified peptide, and the signal was averaged over the chromatographic peak width before superimposition. Overlay (3D) was performed in the Qual Browser (Thermo Fisher Scientific) data viewer followed by spectrum normalization to the largest peak in the scan with multiple scans normalized all the same. (E) Cartoon representation of hTRPA1 structure and approximate location of identified Cys's (red indicates IA adduction). (F) Calculated rate reaction of IA for select hTRPA1 Cys's, indicating the high reactivity of C621.

Covalent modification of C621 in hTRPA1 is >6,000-fold faster than nonreactive Cys

To identify the specific residues rapidly bound by electrophiles, we performed MS analysis of immunoprecipitated hTRPA1 after IA treatment that previously evoked submaximal activation of hTRPA1 (Fig. 2 D). HEK293 cells expressing hTRPA1 were exposed to untagged IA (30 μM, 120 s) and then quenched with 1 mM NEM (7 min). After purification, hTRPA1 was reduced and the remaining Cys's were fully reacted by NMM. Our MS

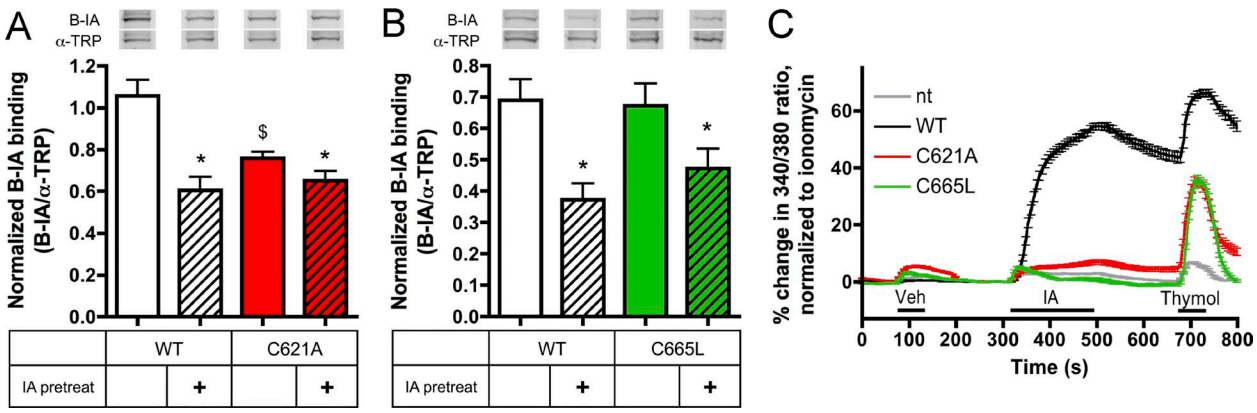

Figure 5. **The role of C621 and C665 in rapid binding and activation of hTRPA1.** (A) Normalized 10 µM B-IA (60 s) binding to hTRPA1 WT (white bars; $n = 7$) and C621A mutant (red bars; $n = 4$). (B) Normalized 10 µM B-IA (60 s) binding to hTRPA1 WT (white bars; $n = 5$) and C665L mutant (green bars; $n = 6$). (A and B) The dollar sign denotes difference from WT ($, $P < 0.05$). Asterisks denotes difference from control (clear bars) with IA pretreatment (100 µM, 10 min; hatched bars; *, $P < 0.05$). Bands in the blots are 131 kD. (C) Activation of TRPA1 constructs (WT, C621A, and C665L) by vehicle (Veh), 30 µM IA, and 200 µM thymol ($n \geq 49$). (A–C) Error bars denote SEM.

analysis detected 768 out of 1,119 residues (Fig. S4). Specifically, we detected 22 out of 28 hTRPA1 Cys's (Fig. 4, A and E), with a mean signal to noise ratio of 543 ± 145. Only four Cys's were reacted by IA (30 µM, 120 s) yielding a CAM modification: C273, C621, C665, and C1085 (Fig. 4, A–D; and Fig. S5). The majority of the other Cys's were modified by NEM (1 mM, 7 min), indicating that these Cys's were also available for electrophilic modification in hTRPA1's native state (Fig. 4 A). Some Cys's, e.g., C173 and C308, were largely modified (by NMM) only after denaturation and reduction. Control experiments with excess IA treatment (not depicted) demonstrated that all 22 detected Cys's were fully modifiable by IA.

C621 was almost completely reacted by IA (97%), whereas only 3–4% of C273, C665, and C1085 were reacted by IA (Fig. 4 A). The C621 peptide also contained C633. Tandem MS (MS/MS) data showed no evidence of IA reaction (CAM modification) with C633 (Fig. 4, B and C): the most intense fragment ion, y5, which contains only C633, would be detected at m/z 664.3 if modified by IA; however, no fragment ion signal at this m/z value was observed in any of the MS/MS spectra. Instead, y5 was detected at m/z 732.3 (Fig. 4 B) and 718.3 (Fig. 4 C), indicating C633 adducted by NEM and NMM, respectively. We compared the IA binding (CAM modification) of Cys with C540, a well-detected residue that had no measurable IA binding. Assuming IA binding was lower than the limit of detection, the K_{obs} for C540 was $<0.16\ M^{-1}s^{-1}$, similar to the calculated second order rates for IA reaction with GSH. K_{obs} for IA reaction with C273, C665, and C1085 was $\sim 11\ M^{-1}s^{-1}$, and the K_{obs} for C621 was $980\ M^{-1}s^{-1}$ (Fig. 4 F). Thus, the reaction of C621 with IA was >6,282-fold quicker than for C540 (Fig. S6). This very rapid modification of C621 is consistent with the second order rate reactions calculated for IA-induced hTRPA1 activation (Fig. 2 F).

To put the kinetics of hTRPA1 electrophilic sensing into context with other characterized electrophilic sensors, we briefly investigated the activation of the nuclear factor erythroid 2–related factor 2 (Nrf2) system, which controls the protective antioxidant response element (ARE) in neurons and other cells (Holland and Fishbein, 2010; Brigelius-Flohé and Flohé, 2011). Electrophiles react with the canonical electrophile sensor Keap1, which then allows the translocation of Nrf2 into the nucleus (Dinkova-Kostova et al., 2002). 30 µM IA for 2 min evoked only a minor response from the Keap1-Nrf2 system (Fig. S7), compared with near maximal response from hTRPA1 (Fig. 2 D), suggesting that functional Cys's in hTRPA1 are more reactive than those in Keap1.

The role of C621 and C665 in electrophilic binding and activation

Using a C621A mutant, we found that the reactive component of B-IA binding was significantly reduced compared with the wild-type channel (Fig. 5 A), confirming that C621 contributes overwhelmingly to rapid modification of hTRPA1 by IA. Unsurprisingly, the C621A mutant was almost completely insensitive to activation by 30 µM IA (Fig. 5 C). A previous study has suggested C665 as critical to hTRPA1 activation by electrophiles (Hinman et al., 2006), and although we observed rapid modification of C665 in our MS experiments, it was limited compared with C621. Consistent with this, we observed little difference in B-IA binding of a C665L mutant compared with wild type (Fig. 5 B), indicating that the majority of reactive Cys modification occurs independently of C665. Nevertheless, the C665L mutant was completely insensitive to activation by 30 µM IA (Fig. 5 C). Such data suggest that C665 plays a critical role in hTRPA1 activation downstream of rapid cova-

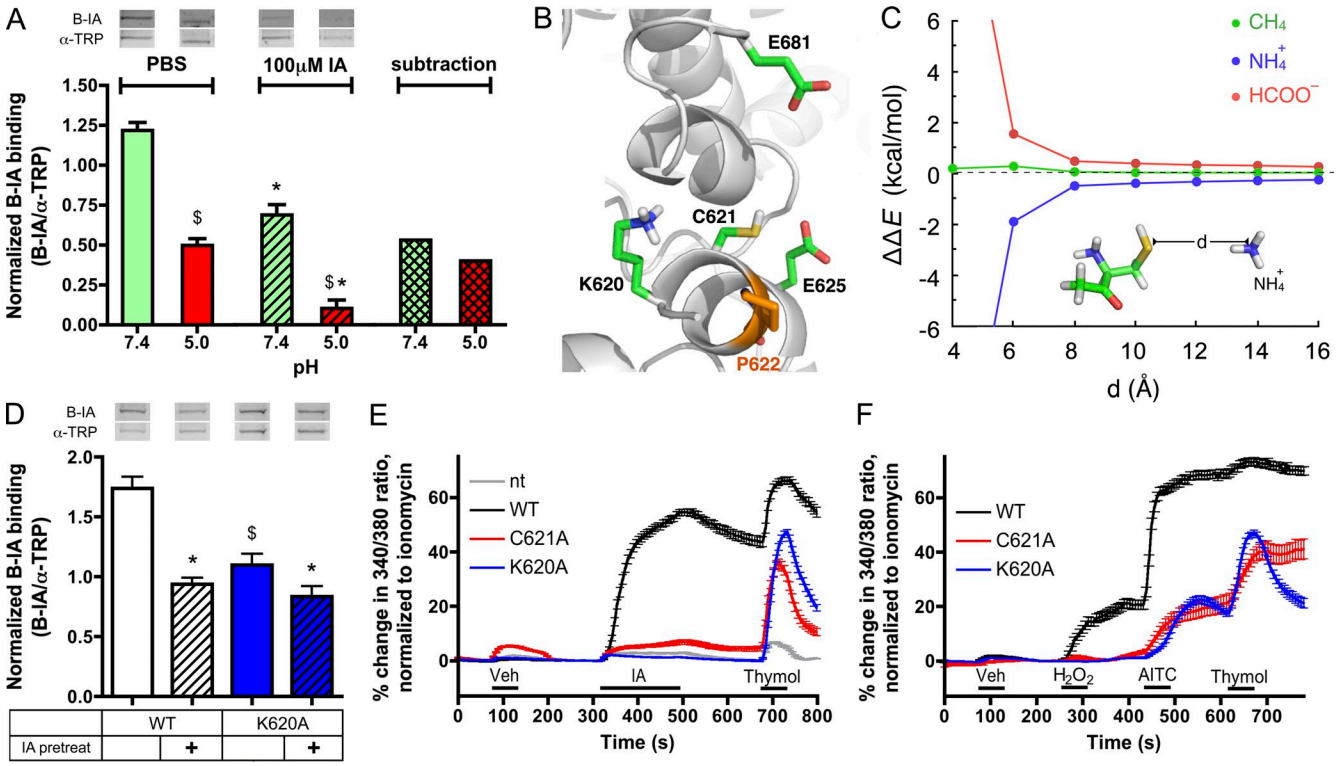

Figure 6. **K620 is required for high reactivity of C621.** (A) Normalized 10 μM B-IA (60 s) binding to hTRPA1 at pH 7.4 (green bars) and 5.0 (red bars) without (clear bars) and with (hatched bars) IA pretreatment (100 μM, 10 min at pH 7.4; $n \geq 3$). Dollar signs denote difference from pH 7.4 with pH 5.0 ($, $P < 0.05$). Asterisks denote difference from control with IA pretreatment (*, $P < 0.05$). IA pretreatment data were subtracted from control to show reactive binding (crosshatched bars). (B) Predicted structure of C621 domain based on Paulsen et al. (2015). (C) Modeling of the change in Cys deprotonation energies ($\Delta\Delta E$) caused by proximity of CH_4, NH_4^+, and $HCOO^-$ groups. (D) Normalized 10 μM B-IA (60 s) binding to hTRPA1 WT (white bars, $n = 6$) and K620A mutant (blue bars, $n = 8$). The dollar sign denotes difference from WT ($, $P < 0.05$). Asterisks denote difference from control (clear bars) with IA pretreatment (100 μM, 10 min; hatched bars; *, $P < 0.05$). (A and D) All bands in the blots are 131 kD. (E) Activation of TRPA1 constructs (WT, C621A, and K620A) by vehicle (Veh), 30 μM IA, and 200 μM thymol ($n \geq 124$). (F) Activation of TRPA1 constructs (WT, C621A, and K620A) by vehicle (Veh), 100 μM H_2O_2, 100 μM AITC, and 200 μM thymol ($n \geq 33$). (A and D–F) Error bars denote SEM.

lent modification of C621. Importantly, both mutants were adequately expressed in HEK293 (Fig. S8) and responded robustly to the non-electrophilic TRPA1 activator thymol (200 μM; Fig. 5 C), suggesting that decrements in either IA binding/activation were caused by specific perturbations rather than a nonspecific inhibition of channel functionality.

K620 is essential for C621 reactivity

The exceptional reactivity of C621 compared with other Cys's implies that C621 is embedded in a unique local environment that lowers its reaction barrier. A major contributor to a cysteine's reaction barrier is its deprotonation energy (Bednar, 1990; Kortemme and Creighton, 1995). The standard aqueous phase pK_a of Cys is 8.5, meaning that ~10% are thiolate at physiological pH. For Cys's whose pK_a is lowered by their local environment, the deprotonation barrier will be relatively smaller at physiological pH, which increases reactivity. We investigated the effect of pH on the B-IA binding of hTRPA1 expressed on HEK293, using saponin to access the intracellular milieu. As expected, decreasing intracellular pH to 5 decreased B-IA total binding, as the result of a decrease in thiolate groups (Fig. 6 A). With HEK293 first pretreated with IA at pH 7.4 (i.e., to bind the reactive groups), decreasing the pH to 5 greatly reduced B-IA binding of the unreactive Cys groups, consistent with their "putative" high pK_a. By subtracting the IA-pretreated groups from the control groups, we resolved the approximate B-IA binding of the reactive groups. Thus, we found that decreasing intracellular pH from 7.4 to 5 had little effect on B-IA binding of reactive groups, suggesting that the proportion of thiolate in these groups is stable at very low pH (Fig. 6 A).

To gain molecular insight into how the local environment may reduce the pK_a of C621, we examined the distribution of acidic and basic residues within 10 Å from C621. The recent 4.2-Å-resolution cryo-EM model of the channel (Paulsen et al., 2015) indicates that C621 is flanked by a pair of proximal basic (K620) and acidic (E625) residues and a more distant E681 (Fig. 6 B). Such a distribution, along with the fact that C621 is partly bur-

ied in a low dielectric environment, suggests that C621 will have a p$K_a \geq 8.5$ (Malmberg et al., 2004; Varma and Jakobsson, 2004). However, we note that the α-helix that contains C621 and E625 also contains an interleaved proline, P622. This proline will either induce a kink in the helix and/or reduce helicity (Gunasekaran et al., 1998), and in both cases, E625 will be pushed away from C621. As a result of this structural change, the positively charged K620 will be closer to C621 compared with the negatively charged glutamates, E625 and E681.

What effect will such structural changes have on C621's pK_a? To gain fundamental insight, we performed a systematic quantum mechanical study of how proximity of representative functional groups (X = {NH_4^+, $HCOO^-$, CH_4}) affects the deprotonation energy of Cys ($\Delta\Delta E$; Fig. 6 C). We note first that even the hydrophobic control group, CH_4, affects $\Delta\Delta E$, although the effect is minor. We attribute this to CH_4's polarizability (Rossi et al., 2013). We note next that when the basic group (NH_4^+) is placed at a distance of 6 Å, which is roughly the distance between C621 and K620 in the cryo-EM model (Paulsen et al., 2015), it reduces the $\Delta\Delta E$ by 1.9 kcal/mol. Assuming that entropic contributions cancel out, such a change in electronic energy corresponds to a drop in 1.4 pK_a units, as $\Delta pK_a = \Delta\Delta G/2.3RT$, where $\Delta\Delta G$ is the corresponding free energy change, R is the gas constant, and T = 298.15 K (Varma and Jakobsson, 2004). We also note a nonlinear dependence of $\Delta\Delta E$ on the Cys–X distance, and as the distance increases beyond 8 Å, the contribution of functional groups to $\Delta\Delta E$ becomes relatively much smaller. Therefore, considering that the interleaved proline P622 likely causes the C621–E625 distance to be greater than the C621–K620 distance, we expect that the pK_a of C621 will be lower than its standard value of 8.5, which would enhance the reactivity of C621.

We tested the contribution of K620 to rapid covalent modification and activation of hTRPA1 by IA using a K620A mutant. Despite the presence of all native Cys residues, the reactive component of B-IA binding was almost abolished in the K620A mutant (Fig. 6 D). Furthermore, the K620A mutant was insensitive to activation by IA (Fig. 6 E), indicating the critical requirement for a coordinated environment at C621 for hTRPA1 sensitivity to IA. Again, the K620A mutant was well expressed (Fig. S8) and responded robustly to thymol (Fig. 6 E). Given that TRPA1 possesses reactive Cys's that appear to have low pK_a and given that K620 likely coordinates the reactivity of C621, we hypothesized that K620 contributes to the capacity for substantial binding of B-IA at low intracellular pH. There was virtually no B-IA binding of the K620A mutant at pH 5.0 (Fig. S9), indicating that K620 likely coordinates C621's reactivity in part through decreasing its pK_a.

We also briefly investigated the contribution of C621 and K620 to hTRPA1 activation by H_2O_2 and allyl isothiocyanate (AITC; Fig. 6 F). Neither the C621A or K620A mutants responded to 100 µM H_2O_2, and both responded weakly to 100 µM AITC, which is thought to directly activate hTRPA1 via Cys residues and K708 (Hinman et al., 2006).

DISCUSSION

The rapid detection of electrophiles is fundamental to TRPA1's role in initiating rapid nociceptive responses to oxidative stress. IA and cinnamaldehyde reacted with conventional thiols at ∼0.1–1 $M^{-1}s^{-1}$ (Jones et al., 1975; Bednar, 1990; Chen and Armstrong, 1995). Here, we show that electrophile-induced TRPA1 activation occurred at 500–900 $M^{-1}s^{-1}$, suggesting exceptional reactivity of functional Cys residues in TRPA1. Previous studies using excess exposures have shown TRPA1 modification by electrophiles and, as a result, multiple TRPA1 Cys's have been implicated (Macpherson et al., 2007a; Wang et al., 2012). Here, using concentrations and exposure times sufficient to cause submaximal TRPA1 activation, we determined two binding populations: a rapidly bound and saturated group and a slowly bound, unsaturated group. The reactive population was detected in hTRPA1 and mTRPA1, both of which are rapidly activated by electrophiles (Jordt et al., 2004; Hinman et al., 2006; Macpherson et al., 2007a), whereas rsTRPA1 had no reactive population, indicating rsTRPA1 insensitivity to electrophiles (Cordero-Morales et al., 2011) is caused by a lack of rapid electrophilic binding.

MS analysis indicated only four TRPA1 Cys residues were modified within the short IA exposure: C273, C621, C665, and C1085. All are intracellular, consistent with reported accessibility requirements for electrophile-induced TRPA1 activation (Macpherson et al., 2007a). In particular, C621 was almost completely modified by IA, making up the majority of rapid TRPA1 modification. None of the other 18 TRPA1 Cys's were modified by IA, although 17 were available for modification in TRPA1's native state. Thus, the selective modification of the four Cys's by brief IA treatment was the result of high reactivity. It is likely that these Cys's represent the population of reactive groups detected in the B-IA binding experiments. This was confirmed by use of the C621A mutant, which displayed greatly reduced B-IA binding.

Pretreatment with nonfluorescent IA (100 µM, 10 min) was estimated to react with ∼10% of free conventional Cys's. Unsurprisingly, this failed to abolish rapid B-IA binding to TRPs. The modification of the nonreactive Cys's was so limited that we failed to detect CAM modifications on 18 of 22 Cys's after rapid IA treatment. The mean signal to noise ratio in the MS analysis was >500, suggesting that IA reacted with <0.2% of these residues, compared with 97% for C621 and 3–4% for C273, C665, and C1085. Therefore, C540 reacted with IA at a rate of <0.16 $M^{-1}s^{-1}$, compared with ∼11 $M^{-1}s^{-1}$ for C273,

C665, and C1085 and 980 $M^{-1}s^{-1}$ for C621. Thus, C621 was modified >6,282 times faster than C540. These rates are consistent throughout our study: the IA reaction rate for C540 in the MS analysis was similar to the rate for conventional Cys's determined spectrophotometrically, and the reaction rate for IA-induced C621 modification in the MS analysis was similar to the rate reaction calculated for IA-induced hTRPA1 activation. Potentially underestimating the rates determined from the cell-based assays is the requirement for IA to first cross the membrane, although this has been previously shown to occur very rapidly at ∼400 nm/s (Sha'afi and Pascoe, 1973).

Our data provide an explanation for the mechanism of hTRPA1 activation by electrophiles. We have shown that electrophilic binding occurs within the time frame of activation and that binding is required for activation. A critical step in rapid binding is modification of C621. The C621A mutant displayed greatly reduced reactive binding of B-IA and was not activated by IA. Interestingly, binding of C621 alone was not sufficient for activation. Although only 4.6% of C665 residues in wild-type hTRPA1 were bound, the mutant C665L was not activated by IA, demonstrating an absolute requirement for C665 in the activation of hTRPA1. Despite evidence of rapid C665 binding, we cannot definitively state that C665 binding specifically is required for activation. Although likely, we have no direct evidence that the hTRPA1 population adducted at C621 overlaps with the population adducted at C665. A substantial proportion of C665 was protected from IA/NEM modification in the native state of the channel, possibly because of C665 involvement in disulfide bonding (Wang et al., 2012). Thus, it is plausible that C621 binding may modulate C665's reactivity, but we presently have no evidence supporting this hypothesis. Intracellular polyphosphates are known to be required for TRPA1 activation by electrophiles (Kim and Cavanaugh, 2007) and have been shown to stabilize the coil-coiled domains in the intracellular C terminus (Paulsen et al., 2015). The presence or absence of polyphosphates had no effect on hTRPA1 binding of B-IA, suggesting that polyphosphates and the stabilized coiled-coil domains are required for processes involved in activation downstream of binding. Unsurprisingly, inhibitors of TRPA1, which block electrophile- and non-electrophile–induced TRPA1 activation, had no effect on rapid binding of TRPA1, thus confirming their role as allosteric channel inhibitors.

The high reactivity of C621 is crucial to subsequent activation by electrophiles. However, there are no known identifying sequences that confer reactivity to Cys (Marino and Gladyshev, 2012). Thiolate is the active moiety; thus, low pK_a can contribute to reactivity. Decreasing the pH to 5 had little effect on B-IA binding of the reactive groups, suggesting a low pK_a compared with conventional Cys. Adjacent to C621 in mammalian TRPA1 is a conserved lysine/arginine, which our quantum mechanical study suggests can significantly lower C621 pK_a, and thereby increase its reactivity. Mutational experiments performed in this study confirm the critical role of K620: the K620A mutant displayed little B-IA reactive binding and was not activated by IA even though all hTRPA1 Cys's were present. Nevertheless, we also note that the reaction rate of completely deprotonated thiolate in GSH with IA is 33 $M^{-1}s^{-1}$ (Bednar, 1990), much slower than the C621 reaction rate. Thus, a low pK_a of C621 alone does not explain fully its high reactivity, and it is possible that the local environment (including K620) participates directly in the reaction of electrophiles with C621.

Our data indicate critical roles of K620 and C621 in rapid electrophilic adduction of hTRPA1 and K620, C621, and C665 in rapid activation of hTRPA1 by electrophiles. Nevertheless, rsTRPA1, which is insensitive to electrophiles, possesses equivalent lysine and cysteine residues (Gracheva et al., 2010; Cordero-Morales et al., 2011). Therefore, the residues identified in this study are not the sole determinants of high reactivity (and subsequent channel activation) to electrophiles. Further work is required to fully identify the reactive Cys motifs in TRPA1.

Previous studies have identified residues important for electrophilic activation of TRPA1. Combined mutation of C621, C641, and C665 abolished hTRPA1 activation by NMM and 4-hydroxynonenal (Hinman et al., 2006; Trevisani et al., 2007). Single mutations of C621 or C414 or C421 also decreased hTRPA1 activation by the electrophile 15d-Prostaglandin J_2 (Takahashi et al., 2008), although the latter two mutants displayed poor overall channel function. Our data are consistent with a role of C621 and C665 in binding and activation. We find no evidence that C414, C421, or C641 is modified by rapid electrophilic treatment, and thus we argue that these residues are not directly involved in binding (although their modification by NMM after reduction suggests disulfide bonding).

To be an effective sensor of electrophiles, TRPA1 must react with electrophiles in the presence of intracellular GSH and enzymes that accelerate GSH-mediated detoxification (Brigelius-Flohé and Flohé, 2011). The exceptionally high reactivity of C621 (980 $M^{-1}s^{-1}$) provides TRPA1 with this critical function. Reactive Cys's are commonly found in antioxidant defense proteins such as thioredoxins and glutaredoxins, which have IA reactions rates <100 $M^{-1}s^{-1}$ (Yang and Wells, 1991; Nelson and Creighton, 1994; Mössner et al., 1998); thus, TRPA1 is able to compete effectively within this environment. This is illustrated by its comparison with electrophilic modulation of Keap1-Nrf2 activity, the canonical electrophile sensor in the ARE system (Holland and Fishbein, 2010), which was barely activated by IA exposures capable of substantial C621 modification and hTRPA1 activation.

In conclusion, TRPA1's function as an initiator of oxidative stress–induced nociception depends on the high reactivity of C621, a property that is dependent on the proximity of K620. Nevertheless, complete binding of C621 is not sufficient for activation, which also depends on the function of the reactive C665. By studying the kinetics of both binding and activation, it may yet be possible to determine the mechanisms underlying the exceptional electrophilic sensitivity of TRPA1.

ACKNOWLEDGMENTS

We would like to thank M. Grass for his help analyzing the Nrf2 immunocytochemistry. We would like to thank E.S. Bennett and R.J. Deschenes for their constructive critiques of this manuscript. We would like to thank D. Julius, A. Patapoutian, and J. Remington for kindly sharing their constructs.

This work was supported by National Heart, Lung, and Blood Institute grants R01HL119802 (to T.E. Taylor-Clark) and R01HL119802S1 (to T.A. Parks).

The authors declare no competing financial interests.

Angus C. Nairn served as editor.

Submitted: 1 February 2016
Accepted: 6 May 2016

REFERENCES

Bandell, M., G.M. Story, S.W. Hwang, V. Viswanath, S.R. Eid, M.J. Petrus, T.J. Earley, and A. Patapoutian. 2004. Noxious cold ion channel TRPA1 is activated by pungent compounds and bradykinin. *Neuron.* 41:849–857. http://dx.doi.org/10.1016/S0896-6273(04)00150-3

Bautista, D.M., S.E. Jordt, T. Nikai, P.R. Tsuruda, A.J. Read, J. Poblete, E.N. Yamoah, A.I. Basbaum, and D. Julius. 2006. TRPA1 mediates the inflammatory actions of environmental irritants and proalgesic agents. *Cell.* 124:1269–1282. http://dx.doi.org/10.1016/j.cell.2006.02.023

Becke, A.D. 1993. Density-functional thermochemistry. III. The role of exact exchange. *J. Chem. Phys.* 98:5648–5652. http://dx.doi.org/10.1063/1.464913

Bednar, R.A. 1990. Reactivity and pH dependence of thiol conjugation to N-ethylmaleimide: detection of a conformational change in chalcone isomerase. *Biochemistry.* 29:3684–3690. http://dx.doi.org/10.1021/bi00467a014

Brigelius-Flohé, R., and L. Flohé. 2011. Basic principles and emerging concepts in the redox control of transcription factors. *Antioxid. Redox Signal.* 15:2335–2381. http://dx.doi.org/10.1089/ars.2010.3534

Cancès, E., B. Mennucci, and J. Tomasi. 1997. A new integral equation formalism for the polarizable continuum model: theoretical background and applications to isotropic and anisotropic dielectrics. *J. Chem. Phys.* 107:3032–3041. http://dx.doi.org/10.1063/1.474659

Chen, J., and R.N. Armstrong. 1995. Stereoselective catalysis of a retro-Michael reaction by class mu glutathione transferases. Consequences for the internal distribution of products in the active site. *Chem. Res. Toxicol.* 8:580–585. http://dx.doi.org/10.1021/tx00046a012

Cordero-Morales, J.F., E.O. Gracheva, and D. Julius. 2011. Cytoplasmic ankyrin repeats of transient receptor potential A1 (TRPA1) dictate sensitivity to thermal and chemical stimuli. *Proc. Natl. Acad. Sci. USA.* 108:E1184–E1191. http://dx.doi.org/10.1073/pnas.1114124108

Dinkova-Kostova, A.T., W.D. Holtzclaw, R.N. Cole, K. Itoh, N. Wakabayashi, Y. Katoh, M. Yamamoto, and P. Talalay. 2002. Direct evidence that sulfhydryl groups of Keap1 are the sensors regulating induction of phase 2 enzymes that protect against carcinogens and oxidants. *Proc. Natl. Acad. Sci. USA.* 99:11908–11913. http://dx.doi.org/10.1073/pnas.172398899

Dooley, C.T., T.M. Dore, G.T. Hanson, W.C. Jackson, S.J. Remington, and R.Y. Tsien. 2004. Imaging dynamic redox changes in mammalian cells with green fluorescent protein indicators. *J. Biol. Chem.* 279:22284–22293. http://dx.doi.org/10.1074/jbc.M312847200

Doorn, J.A., and D.R. Petersen. 2002. Covalent modification of amino acid nucleophiles by the lipid peroxidation products 4-hydroxy-2-nonenal and 4-oxo-2-nonenal. *Chem. Res. Toxicol.* 15:1445–1450. http://dx.doi.org/10.1021/tx025590o

Gracheva, E.O., N.T. Ingolia, Y.M. Kelly, J.F. Cordero-Morales, G. Hollopeter, A.T. Chesler, E.E. Sánchez, J.C. Perez, J.S. Weissman, and D. Julius. 2010. Molecular basis of infrared detection by snakes. *Nature.* 464:1006–1011. http://dx.doi.org/10.1038/nature08943

Gunasekaran, K., H.A. Nagarajaram, C. Ramakrishnan, and P. Balaram. 1998. Stereochemical punctuation marks in protein structures: glycine and proline containing helix stop signals. *J. Mol. Biol.* 275:917–932. http://dx.doi.org/10.1006/jmbi.1997.1505

Halliwell, B. 1999. Antioxidant defence mechanisms: from the beginning to the end (of the beginning). *Free Radic. Res.* 31:261–272. http://dx.doi.org/10.1080/10715769900300841

Han, J., C. Clark, G. Han, T.C. Chu, and P. Han. 1999. Preparation of 2-nitro-5-thiobenzoic acid using immobilized Tris(2-carboxyethyl)phosphine. *Anal. Biochem.* 268:404–407. http://dx.doi.org/10.1006/abio.1998.3054

Hayes, J.D., J.U. Flanagan, and I.R. Jowsey. 2005. Glutathione transferases. *Annu. Rev. Pharmacol. Toxicol.* 45:51–88. http://dx.doi.org/10.1146/annurev.pharmtox.45.120403.095857

Hinman, A., H.H. Chuang, D.M. Bautista, and D. Julius. 2006. TRP channel activation by reversible covalent modification. *Proc. Natl. Acad. Sci. USA.* 103:19564–19568. http://dx.doi.org/10.1073/pnas.0609598103

Holland, R., and J.C. Fishbein. 2010. Chemistry of the cysteine sensors in Kelch-like ECH-associated protein 1. *Antioxid. Redox Signal.* 13:1749–1761. http://dx.doi.org/10.1089/ars.2010.3273

Jamur, M.C., and C. Oliver. 2010. Permeabilization of cell membranes. *Methods Mol. Biol.* 588:63–66. http://dx.doi.org/10.1007/978-1-59745-324-0_9

Jones, J.G., S. Otieno, E.A. Barnard, and A.K. Bhargava. 1975. Essential and nonessential thiols of yeast hexokinase. Reactions with iodoacetate and iodoacetamide. *Biochemistry.* 14:2396–2403. http://dx.doi.org/10.1021/bi00682a020

Jordt, S.E., D.M. Bautista, H.H. Chuang, D.D. McKemy, P.M. Zygmunt, E.D. Högestätt, I.D. Meng, and D. Julius. 2004. Mustard oils and cannabinoids excite sensory nerve fibres through the TRP channel ANKTM1. *Nature.* 427:260–265. http://dx.doi.org/10.1038/nature02282

Kim, D., and E.J. Cavanaugh. 2007. Requirement of a soluble intracellular factor for activation of transient receptor potential A1 by pungent chemicals: role of inorganic polyphosphates. *J. Neurosci.* 27:6500–6509. http://dx.doi.org/10.1523/JNEUROSCI.0623-07.2007

Kortemme, T., and T.E. Creighton. 1995. Ionisation of cysteine residues at the termini of model α-helical peptides. Relevance to unusual thiol pK_a values in proteins of the thioredoxin family. *J. Mol. Biol.* 253:799–812. http://dx.doi.org/10.1006/jmbi.1995.0592

Lee, C., W. Yang, and R.G. Parr. 1988. Development of the Colle-Salvetti correlation-energy formula into a functional of the electron density. *Phys. Rev. B Condens. Matter.* 37:785–789. http://dx.doi.org/10.1103/PhysRevB.37.785

Macpherson, L.J., A.E. Dubin, M.J. Evans, F. Marr, P.G. Schultz, B.F. Cravatt, and A. Patapoutian. 2007a. Noxious compounds activate TRPA1 ion channels through covalent modification of cysteines. *Nature.* 445:541–545. http://dx.doi.org/10.1038/nature05544

Macpherson, L.J., B. Xiao, K.Y. Kwan, M.J. Petrus, A.E. Dubin, S. Hwang, B. Cravatt, D.P. Corey, and A. Patapoutian. 2007b. An ion channel essential for sensing chemical damage. *J. Neurosci.* 27:11412–11415. http://dx.doi.org/10.1523/JNEUROSCI.3600-07.2007

Malmberg, N.J., S. Varma, E. Jakobsson, and J.J. Falke. 2004. Ca^{2+} activation of the $cPLA_2$ C2 domain: ordered binding of two Ca^{2+} ions with positive cooperativity. *Biochemistry.* 43:16320–16328. http://dx.doi.org/10.1021/bi0482405

Marino, S.M., and V.N. Gladyshev. 2012. Analysis and functional prediction of reactive cysteine residues. *J. Biol. Chem.* 287:4419–4425. http://dx.doi.org/10.1074/jbc.R111.275578

Marnett, L.J., J.N. Riggins, and J.D. West. 2003. Endogenous generation of reactive oxidants and electrophiles and their reactions with DNA and protein. *J. Clin. Invest.* 111:583–593. http://dx.doi.org/10.1172/JCI200318022

Mendoza, V.L., and R.W. Vachet. 2009. Probing protein structure by amino acid-specific covalent labeling and mass spectrometry. *Mass Spectrom. Rev.* 28:785–815. http://dx.doi.org/10.1002/mas.20203

Montgomery, J.A., J.W. Ochterski, M.J. Frisch, and G.A. Petersson. 1999. A complete basis set model chemistry. VI. Use of density functional geometries and frequencies. *J. Chem. Phys.* 110:2822–2827. http://dx.doi.org/10.1063/1.477924

Mössner, E., M. Huber-Wunderlich, and R. Glockshuber. 1998. Characterization of *Escherichia coli* thioredoxin variants mimicking the active-sites of other thiol/disulfide oxidoreductases. *Protein Sci.* 7:1233–1244. http://dx.doi.org/10.1002/pro.5560070519

Nassenstein, C., K. Kwong, T. Taylor-Clark, M. Kollarik, D.M. Macglashan, A. Braun, and B.J. Undem. 2008. Expression and function of the ion channel TRPA1 in vagal afferent nerves innervating mouse lungs. *J. Physiol.* 586:1595–1604. http://dx.doi.org/10.1113/jphysiol.2007.148379

Nelson, J.W., and T.E. Creighton. 1994. Reactivity and ionization of the active site cysteine residues of DsbA, a protein required for disulfide bond formation in vivo. *Biochemistry.* 33:5974–5983. http://dx.doi.org/10.1021/bi00185a039

Paulsen, C.E., J.P. Armache, Y. Gao, Y. Cheng, and D. Julius. 2015. Structure of the TRPA1 ion channel suggests regulatory mechanisms. *Nature.* 520:511–517. http://dx.doi.org/10.1038/nature14367

Rossi, M., A. Tkatchenko, S.B. Rempe, and S. Varma. 2013. Role of methyl-induced polarization in ion binding. *Proc. Natl. Acad. Sci. USA.* 110:12978–12983. http://dx.doi.org/10.1073/pnas.1302757110

Sha'afi, R.I., and E. Pascoe. 1973. Further studies of sodium transport in feline red cells. *J. Gen. Physiol.* 61:709–726. http://dx.doi.org/10.1085/jgp.61.6.709

Takahashi, N., Y. Mizuno, D. Kozai, S. Yamamoto, S. Kiyonaka, T. Shibata, K. Uchida, and Y. Mori. 2008. Molecular characterization of TRPA1 channel activation by cysteine-reactive inflammatory mediators. *Channels (Austin).* 2:287–298. http://dx.doi.org/10.4161/chan.2.4.6745

Taylor-Clark, T.E., M.A. McAlexander, C. Nassenstein, S.A. Sheardown, S. Wilson, J. Thornton, M.J. Carr, and B.J. Undem. 2008a. Relative contributions of TRPA1 and TRPV1 channels in the activation of vagal bronchopulmonary C-fibres by the endogenous autacoid 4-oxononenal. *J. Physiol.* 586:3447–3459. http://dx.doi.org/10.1113/jphysiol.2008.153585

Taylor-Clark, T.E., B.J. Undem, D.W. Macglashan Jr., S. Ghatta, M.J. Carr, and M.A. McAlexander. 2008b. Prostaglandin-induced activation of nociceptive neurons via direct interaction with transient receptor potential A1 (TRPA1). *Mol. Pharmacol.* 73:274–281. http://dx.doi.org/10.1124/mol.107.040832

Taylor-Clark, T.E., S. Ghatta, W. Bettner, and B.J. Undem. 2009. Nitrooleic acid, an endogenous product of nitrative stress, activates nociceptive sensory nerves via the direct activation of TRPA1. *Mol. Pharmacol.* 75:820–829. http://dx.doi.org/10.1124/mol.108.054445

Taylor-Clark, T.E., K.Y. Wu, J.A. Thompson, K. Yang, P.K. Bahia, and J.M. Ajmo. 2015. Thy1.2 YFP-16 transgenic mouse labels a subset of large-diameter sensory neurons that lack TRPV1 expression. *PLoS One.* 10:e0119538. http://dx.doi.org/10.1371/journal.pone.0119538

Trevisani, M., J. Siemens, S. Materazzi, D.M. Bautista, R. Nassini, B. Campi, N. Imamachi, E. Andrè, R. Patacchini, G.S. Cottrell, et al. 2007. 4-Hydroxynonenal, an endogenous aldehyde, causes pain and neurogenic inflammation through activation of the irritant receptor TRPA1. *Proc. Natl. Acad. Sci. USA.* 104:13519–13524. http://dx.doi.org/10.1073/pnas.0705923104

Varma, S., and E. Jakobsson. 2004. Ionization states of residues in OmpF and mutants: effects of dielectric constant and interactions between residues. *Biophys. J.* 86:690–704. http://dx.doi.org/10.1016/S0006-3495(04)74148-X

Wang, L., T.L. Cvetkov, M.R. Chance, and V.Y. Moiseenkova-Bell. 2012. Identification of in vivo disulfide conformation of TRPA1 ion channel. *J. Biol. Chem.* 287:6169–6176. http://dx.doi.org/10.1074/jbc.M111.329748

Yang, Y.F., and W.W. Wells. 1991. Identification and characterization of the functional amino acids at the active center of pig liver thioltransferase by site-directed mutagenesis. *J. Biol. Chem.* 266:12759–12765.